IOP Conf. Series: Materials Science and Engineering **418** (2018) 012050 doi:10.1088/1757-899X/418/1/012050

# Plastic instabilities in AA5754-O under various stress states

**Yong Hou[1], Junying Min[1,*], Jianping Lin[1,*], John E. Carsley[2] and Thomas B. Stoughton[2]**

[1]School of Mechanical Engineering, Tongji University, Shanghai 201804, China
[2]General Motors Global Research & Development, Warren, MI 48092-2031, USA

*junying.min@tongji.edu.cn (J. Min), jplin58@tongji.edu.cn (J. Lin)

**Abstract**. Spatio-temporal characteristics of plastic instabilities in the aluminium alloy sheet AA5754-O were investigated under three different stress states: uniaxial tension, plane strain and equi-biaxial tension. Tensile tests including conventional uniaxial tensile specimens as well as optimized ISO 16842 cruciform specimens for plane strain and equi-biaxial tensile deformation conditions were carried out at room temperature. Arm strength of the cruciform specimens was enhanced by laser deposition of thickening layers using Al-Mg alloy wire material in order to delay fracture and extend the equivalent plastic strain in the gauge area of the cruciform specimens from ~0.03 to ~0.13 under plane strain condition and to ~0.07 under equi-biaxial tension. The differences in serrated flow behaviour and spatio-temporal evolution of Portevin–Le Châtelier (PLC) bands under these three stress states were investigated using digital image correlation (DIC) techniques. The originality of this paper is to present different PLC phenomena under plane strain condition and equi-biaxial tension, which requires improved models or modifications of existing theoretical frameworks for uniaxial tension to account for different characteristics of PLC phenomena under plane strain and equi-biaxial tension of Al-Mg alloy sheets.

## 1. Introduction

Plastic instabilities attributed to dynamic strain ageing (DSA) are commonly observed during plastic deformation of Al-Mg alloy sheets [1-2] and manifested by surface quality issues on formed components and the propagation of localized deformation bands, referred to as Portevin–Le Châtelier (PLC) bands. Serrated flow behavior in hardening curves are associated with the propagation of the PLC bands and localization of intense dislocation activity within those PLC bands. Generally, PLC bands can be classified into three types based on their different spatio-temporal behavior: Type A (propagating bands with the highest degree of spatial correlation), Type B (hopping or "relay-race" bands [3]), and Type C (static bands) [4]. PLC band behavior has been studied for decades. Sarmah et al. [5] investigated the correlation between the band propagation property and the nature and amplitude of serrations in the Portevin–Le Châtelier effect. It is found that spatial and temporal correlations continuously increase with strain rate from Type C to Type A bands. Although many studies on the occurrence of PLC bands and spatio-temporal characteristics of plastic instabilities in Al-Mg alloy sheets have been reported, this phenomenon has been primarily studied under uniaxial tension deformation and little information has been reported for other strain paths. Manach et al. [6] highlighted the influences of strain rate and temperature on the occurrence of plastic instabilities in simple shear, where they observed plastic instabilities between room temperature and 100 ℃. However, the occurrence of plastic instabilities at

150 ℃ appears to depend on the strain rate. Crescent-shaped plastic instabilities have been observed in hydraulic bulge testing of AA5182-O sheet by Min et al. [7], which are quite different from those observed in uniaxial tensile testing. Recently, PLC bands under plane strain in AlMg3 sheet have been studied by Sene et al. [8] in notched specimen tensile testing. It is noted that no propagation of PLC bands were observed during the notched specimen tensile testing because any PLC effect seems to be constrained by the two notches of the specimen, where localization appears to be dominated by only one single band. Hence, experimental data including serrated flow curves with the propagation of PLC bands remain deficient for alternate strain paths, i.e. plane strain and biaxial tension in the plane stress state, which is very important for the validation of existing theoretical models to predict the occurrence and behavior of such plastic instabilities.

In the present work, cruciform biaxial tensile tests with modified ISO 16842 [9] specimens were used to investigate plastic instabilities of AA5754-O sheet under plane strain and biaxial tension with the aid of digital image correlation (DIC) techniques. Compelling differences were revealed in the spatio-temporal characteristics of plastic instabilities under uniaxial tension, plane strain and biaxial tension by comparing the serrated flow curves and the DIC-computed strain rate contours. The different PLC phenomena under these three strain paths requires improved models or modifications of existing theoretical frameworks to support accurate simulation of Al-Mg alloy sheets.

## 2. Experimental details

The material studied in this work is aluminum alloy AA5754-O with a nominal thickness of 2.0 mm and chemical composition listed in Table 1. Uniaxial tensile specimens following ASTM B557M.9023-1 with a parallel gauge length of 75 mm and a gauge width of 12.5 mm were prepared by wire-electrode cutting at 0 °, 45 ° and 90 ° to the rolling direction, namely, RD, DD and TD. Uniaxial tensile tests were conducted on a MTS E45.105 Universal Testing Machine under displacement control mode with a quasi-static strain rate of ~8.2 $\times 10^{-4}$ $s^{-1}$ at room temperature. Plastic deformation in the gauge area of a cruciform specimen following ISO 16842 is limited when premature fracture occurs on one arm of the specimen during the biaxial tensile tests. In this work, a new method to enhance arm strength was proposed to increase plastic deformation in the gauge area of ISO 16842 cruciform specimen. Slit arms of cruciform specimens of AA5754-O were strengthened using laser deposition of Al-Mg alloy wires having a diameter of ~0.3 mm on both sides, in which the arm is thickened by ~0.5 mm as shown in Figure 1.

**Table 1**. Chemical composition of AA5754-O (wt. %).

| Al | Mg | Mn | Fe | Si | Cu |
|---|---|---|---|---|---|
| Balance | 3.0 | 0.24 | 0.26 | 0.03 | 0.02 |

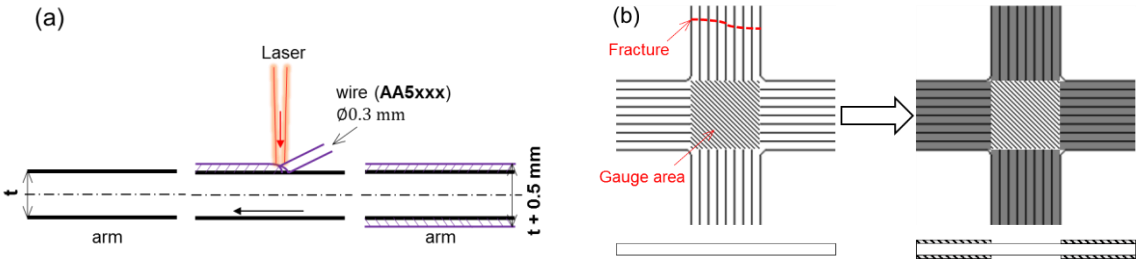


**Figure 1**. (a) Illustration of the laser deposition method, (b) cruciform specimen before and after applying the laser deposition method to strengthen the arms.

Furthermore, the slit geometry in the arms was adjusted to reduce the stress concentration at the end of slits in order to delay fracture. Figure 2 presents the dimensions of the ISO 16842 cruciform specimen as well as specimens with optimized slit dimensions and laser deposition for the load ratios of 1:2 (close to plane strain) and of 1:1 (equi-biaxial tension), which are hereafter designated as X1Y2 specimen and X1Y1 specimen, respectively. The heat-affected zone caused by laser deposition was limited and its

effect on mechanical properties within the gauge area material can be ignored. Biaxial tensile tests of the newly designed cruciform specimens were carried out on a biaxial testing system MTS BIA5105 under load control mode, which means the loading rate is constant during testing at room temperature. Cruciform specimens were positioned in the testing system with RD and TD along the X-axis and Y-axis (refer to Figure 2c), respectively.

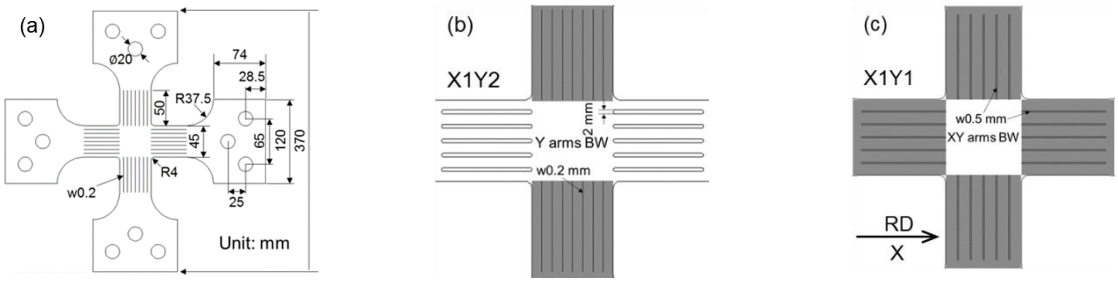


**Figure 2**. (a) Dimensions of the cruciform specimen following ISO 16842, cruciform specimens (b) with Y direction arms built up for load ratio of 1:2 (close to plane strain) and (c) with X and Y direction arms built up for load ratio of 1:1 (equi-biaxial tension).

DIC techniques were applied to obtain full field strain measurements of specimens in uniaxial tension and biaxial (cruciform) tension testing. The speckle pattern for DIC calculation was applied to all specimens and detailed procedures can be found in the literature [10-11].

## 3. Results and discussion

### *3.1. Hardening behaviour of AA5754-O under three stress states*

Initial focus was put on the strain paths of uniaxial tensile specimens along RD, DD and TD and cruciform specimens plotted in Figure 3a. The strain path of X1Y2 specimen is very close to plane strain, while the strain path of X1Y1 specimen deviates slightly from the purely balanced biaxial path. This deviation of strain paths may be related to the anisotropic plastic behavior of the AA5754-O sheet along with test control by loading ratio rather than using feedback control of strain or displacement measurement. For simplicity, the X1Y2 specimens and X1Y1 specimens are hereafter deemed to be deformed under plane stain and equi-biaxial tension, respectively. Stress and plastic strain components of the tested specimens (uniaxial tensile specimens and cruciform specimens) were calculated from the load data and DIC data according to the procedure proposed by Min et al. [10]. The von Mises stresses and equivalent plastic strains were derived from the stress and plastic strain components. The von Mises stress vs. equivalent plastic strain curves under uniaxial tension, plane strain and equi-biaxial tension are compared in Figure 3b and 3c. The measureable equivalent plastic strain in the gauge area of cruciform specimens was increased by the applied laser deposition method up to ~0.131 under plane strain and up to 0.072 under equi-biaxial tension according to Figure 3c. The Hockett-Sherby hardening law expressed by Equation (1) was used to fit the flow curves under these three stress states with parameters of the Hockett-Sherby hardening law listed in Table 2. It can be observed that the fitted curves (dotted curves in Figure 3b and 3c) correlate well with experimental data (solid curves in Figure 3b and 3c).

$$\sigma_{\mathrm{vM}}\left(\overline{\varepsilon_{\mathrm{p}}}\right) = A_{\sigma} - B_{\sigma}\exp\left(-C_{\sigma}\overline{\varepsilon_{\mathrm{p}}}^{b_{\sigma}}\right) \quad (1)$$

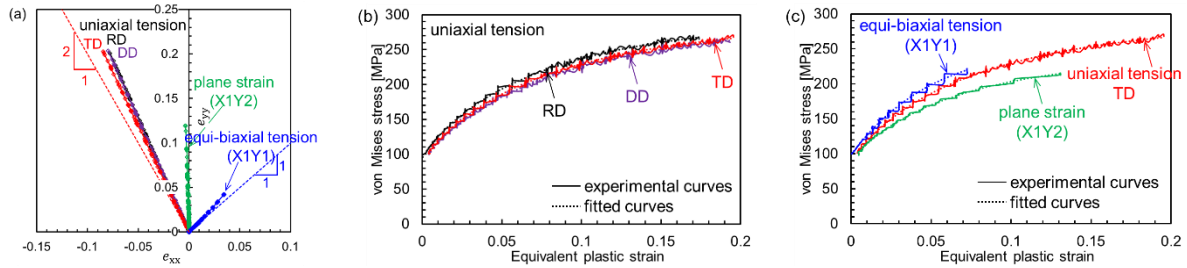


**Figure 3**. (a) Strain paths of uniaxial tensile specimens along RD, DD and TD and cruciform specimens and (b) von Mises stress vs. equivalent plastic strain curves under uniaxial tension along RD, DD and TD, (c) under plane strain and equi-biaxial tension.

**Table 2**. Fitted parameters in the Hockett-Sherby hardening law (Eq. (1)).

| Orientation or stress states | $A_\sigma$ [MPa] | $B_\sigma$ [MPa] | $C_\sigma$ | $b_\sigma$ | $R^2$-value |
|---|---|---|---|---|---|
| UT-RD (uniaxial tension) | 293.3 | 199.5 | 9.37 | 0.8700 | 0.9965 |
| UT-DD (uniaxial tension) | 291.3 | 203.8 | 8.09 | 0.8539 | 0.9960 |
| UT-TD (uniaxial tension) | 291.2 | 206.3 | 8.23 | 0.8350 | 0.9951 |
| X1Y2 (plane strain) | 240.6 | 152.3 | 10.54 | 0.8754 | 0.9978 |
| X1Y1 (equi-biaxial tension) | 255.4 | 156.4 | 22.31 | 1.0326 | 0.9928 |

### *3.2. Spatio-temporal characteristics of plastic instabilities under various stress states*

The true stress vs. true strain curves from uniaxial tensile tests are shown in Figure 4a, where all three curves display evident serrations during plastic deformation. Yield point elongation (YPE) with initial yield stress of ~98 MPa is followed by stress serrations during hardening under uniaxial tension along DD and TD, while YPE does not appear in the hardening curve along RD. This difference in YPE phenomenon along three directions is shown clearly in Figure 4b, and it may be linked to anisotropy of the static strain aging effect. A critical true strain $\varepsilon_C$ was identified at a point where the types of serrations display an easily recognizable change from Type A to Type B based on analysis of stress drops, which is also correlated to the spatial characteristics of PLC bands. $\varepsilon_C$ for uniaxial tension along RD, DD and TD were determined as ~0.041, ~0.048 and ~0.042 (refer to Figure 4c), respectively.

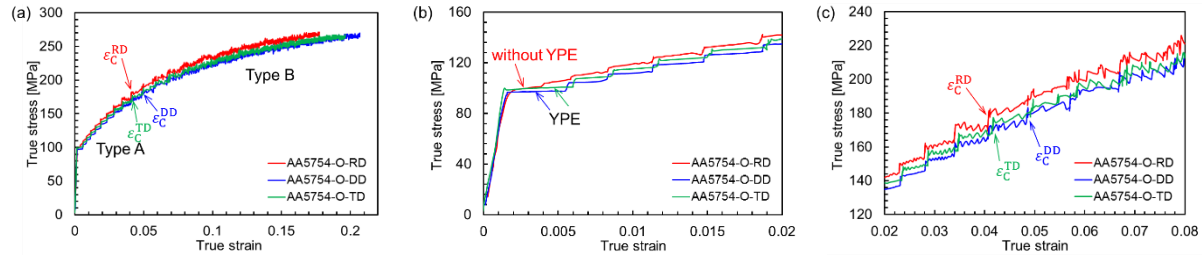


**Figure 4**. True stress vs. true strain curves under uniaxial tension along RD, DD and TD.

It's noted that the direction of the major strain is parallel to TD (Y-axis) of the sheet specimens when testing the X1Y2 cruciform specimens according to the assembly rules. Hence, the von Mises stress vs. equivalent plastic strain curve under uniaxial tension along TD was compared with that under plane strain along TD (X1Y2) and equi-biaxial tension (X1Y1) in Figure 5a. It is clear that all three von Mises stress vs. equivalent plastic strain curves show serrations during plastic deformation. However, some temporal characteristics are different among these three stress states. First, YPE phenomenon appears in the curves under uniaxial tension (TD) and plane strain (TD), while, YPE is not observed under equi-biaxial tension even though AA5754-O exhibits almost the same yield strength of ~98 MPa under these three different stress states. Second, a crossover of Type A serrations (ten step-wise serrations shown in Figure 5b after YPE phenomenon) to Type B serrations was observed under uniaxial tension along TD, while serrations with very low amplitudes appear in the curve under plane strain (TD). It's astonishing

that AA5754-O exhibits typical Type A serrated flow behavior only after the equivalent plastic strain surpasses a critical level of ~0.01 ($\varepsilon_S$ in Figure 5a) when the gauge area of the cruciform specimens was deformed under in-plane equi-biaxial tension. Similar serrated flow behavior was observed at the pole of specimens in hydraulic bulge deformation of AA5182-O sheet under balanced biaxial tension, where serrations were only observed to occur in the flow curves beyond a critical equivalent strain for all bulge tests [7]. These differences in serrated flow curves under uniaxial tension, plane strain and equi-biaxial tension are related to the stress states (uniaxial tension, plane strain and equi-biaxial tension), specimen geometry (dog bone specimens or cruciform specimens) and control mode (displacement control or load control) in the tests. The correlated spatial characteristics of plastic instabilities under these three stress states were presented in next paragraphs.

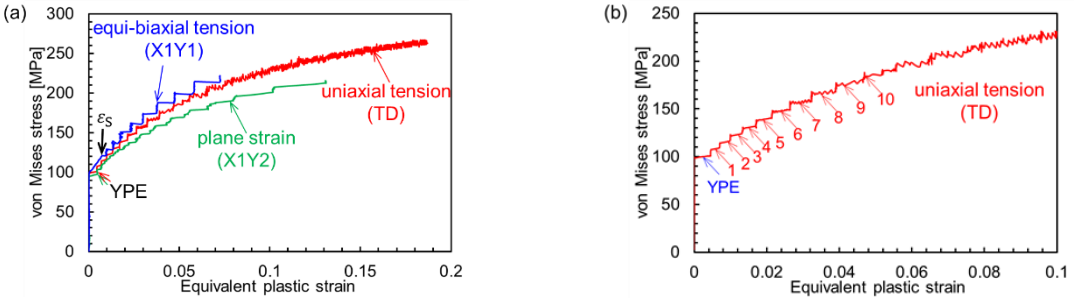


**Figure 5**. Von Mises stress vs. equivalent plastic strain curves under uniaxial tension along TD, plane strain along TD and equi-biaxial tension.

The contour of $\dot{e}_{yy}$, true strain rate in Y direction, in the uniaxial tensile specimen along TD at the last frame before fracture is shown in Figure 6a, in which A is the point with the maximum strain rate at this frame, and O is the geometrical center of the uniaxial tensile specimen. Figure 6b shows the temporal evolution of $\dot{e}_{yy}$(A), true strain rate in Y direction at A point (blue solid), $e_{yy}$(A), true strain in Y direction at A point (red solid) and $e_{yy}$(O), true strain in Y direction at O point (red dashed), where spikes in $\dot{e}_{yy}$(A) curve (blue solid) are coincident with step-wise increases in $e_{yy}$(A) curve (red solid). The temporal evolution of $\dot{e}_{yy}$ contours of the uniaxial tensile specimen along TD is shown in Figure 6c, where yellow or red contours denote the peak strain rates associated with PLC bands. The true strain rate was extracted from the central line with a length of ~100 mm along the axial direction of specimen as illustrated by the yellow solid line in Figure 6a. Localized band, named Lüders band, propagates from the top end to the bottom end of the uniaxial tensile specimen during the YPE phenomenon at the beginning of plastic deformation coincident with the first spike in $\dot{e}_{yy}$(A) curve (blue solid) in Figure 6b. The YPE phenomenon is followed by ten sets of PLC bands which propagate regularly in the uniaxial tensile specimen before the time of ~66.6 s ($t_1$ in Figure 6b and 6c) corresponding to $\varepsilon_C^{TD}$ of ~0.042 in Figure 4c, and these PLC bands over this period are classified as Type-A bands. These ten sets of PLC bands are temporally coincident with the ten spikes in $\dot{e}_{yy}$(A) curve before the first black dashed line $t_1$ in Figure 6b, and are also temporally coincident with the ten step-wise serrations marked by numbers in the von Mises stress vs. equivalent plastic strain curve in Figure 5b. After this moment ($t_1$), there are several hopping propagations of PLC bands corresponding to Type B serrations in Figure 4a before the time of ~200 s ($t_2$ in Figure 6b and 6c). After the hopping propagations, the PLC bands start to localize around the position of Y = ~28.2 mm until fracture occurred.

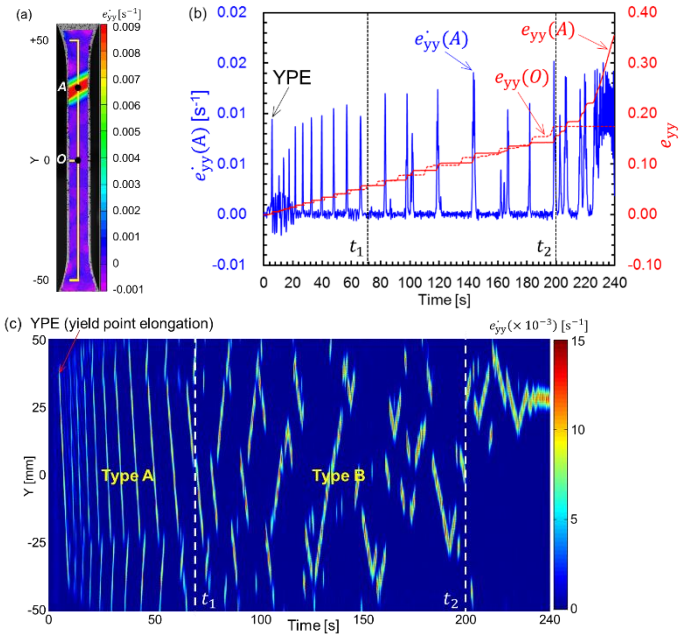


**Figure 6**. (a) The $\dot{e}_{yy}$ contour of the uniaxial tensile specimen at last frame before fracture. (b) The temporal evolution of $\dot{e}_{yy}$ and $e_{yy}$ at point A and point O. (c) The evolution of $\dot{e}_{yy}$ contours under uniaxial tension along TD.

The temporal evolution of $\dot{e}_{yy}$, true strain rate (blue solid) in Y direction and $e_{yy}$, true strain (red solid) in Y direction at the geometrical point of X1Y2 specimen are shown in Figure 7a. A small spike was observed in the $\dot{e}_{yy}$ curve (blue solid curve in Figure 7a) at the beginning of plastic deformation under plane strain in Figure 7a and 7b, which is coincident with the first step-wise increase of the $e_{yy}$ curve (red solid curve) in Figure 7a. The load control mode results in a continuous increase in amplitude of the $\dot{e}_{yy}$ spikes, which is clearly shown in Figure 7b. To investigate the spatial characteristics of plastic instabilities under plane strain, the evolution of $\dot{e}_{yy}$ contour along the geometrical central lines of X1Y2 specimen in Y direction and in X direction are shown in Figure 7c and 7d, respectively, in which the propagation of PLC bands was firstly observed under plane strain along these two orthogonal directions. The color of the $\dot{e}_{yy}$ contours from 0 s to 110 s is almost uniform and dark blue, which suggests no PLC effect within the elastic stage; therefore, the $\dot{e}_{yy}$ contours from 0 s to 110 s are not included in Figure 7c and 7d. The first localized band, named Lüders band was observed to occur at the time of ~125 s correlated to the YPE features in Figure 7a, and the Lüders band as well as the following five PLC bands are not clearly spatially correlated, denoted as non-matured localized bands. However, PLC bands become more and more mature and are clearly spatially correlated with the continuous increase in amplitude of the true strain rate spikes. All of the PLC band propagations in Figure 7c and 7d correlated to the serrations with very low amplitudes appeared in the von Mises stress vs. equivalent plastic strain curve under plane strain (TD) in Figure 5a.

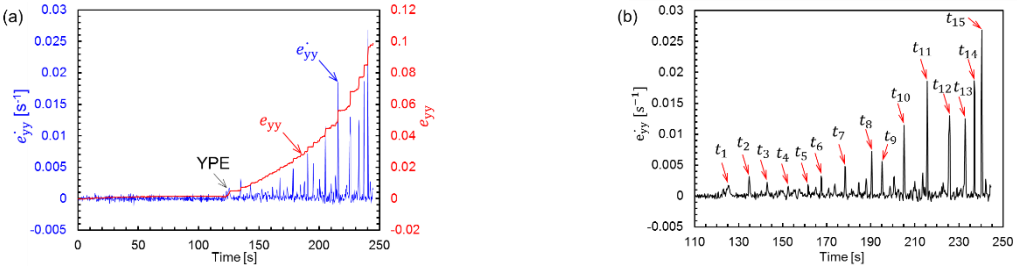

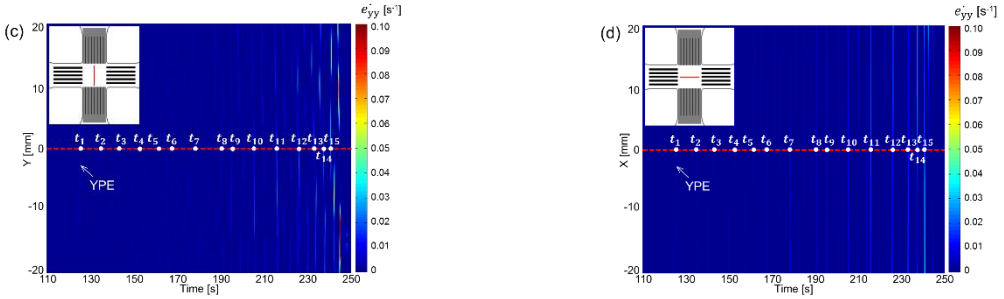


**Figure 7**. (a) The temporal evolution of $\dot{e}_{yy}$ and $e_{yy}$ at the geometrical point of cruciform specimen under plane stain state. (b) Spikes in the evolution of $\dot{e}_{yy}$. (c) The evolution of $\dot{e}_{yy}$ contours along the geometrical central line in Y direction and (d) X direction under plane strain.

The temporal evolution of $\dot{\bar{\varepsilon}}$, equivalent strain rate (blue solid) and $\bar{\varepsilon}$, equivalent strain (red solid) at the geometrical center of X1Y1 specimen are shown in Figure 8a. The similar phenomenon that strain rate increases during the tensile tests is observed under equi-biaxial tension (X1Y1 specimen) as that occurred in the biaxial tensile tests of X1Y2 specimen under load control mode as shown in Figure 8b. The amplitude of step-wise increase in $\bar{\varepsilon}$ curve (red solid) under equi-biaxial tension is larger than that under plane strain, which is related to the typical Type A serrated flow curve under equi-biaxial tension in Figure 5a. The evolution of $\dot{\bar{\varepsilon}}$ contours along the geometrical central lines of X1Y1 specimen in Y direction and in X direction are shown in Figure 8c and 8d, respectively, in which eleven matured PLC bands are clearly observed coincident with eleven typical step-wise increases in the $\bar{\varepsilon}$ curve and eleven large spikes in the $\dot{\bar{\varepsilon}}$ curve in Figure 8a. The colour of $\dot{\bar{\varepsilon}}$ contours from 0 s to 130 s is almost uniform and dark blue because no PLC effect occurs before the equivalent plastic strain surpasses a critical level of ~0.01 ($\varepsilon_S$in Figure 5a); therefore, the $\dot{\bar{\varepsilon}}$ contours from 0 s to 130 s are not included in Figure 8c and 8d. The PLC band propagations in Figure 8c and 8d are highly correlated to the Type A serrations in the von Mises stress vs. equivalent plastic strain curve under equi-biaxial tension in Figure 5a.

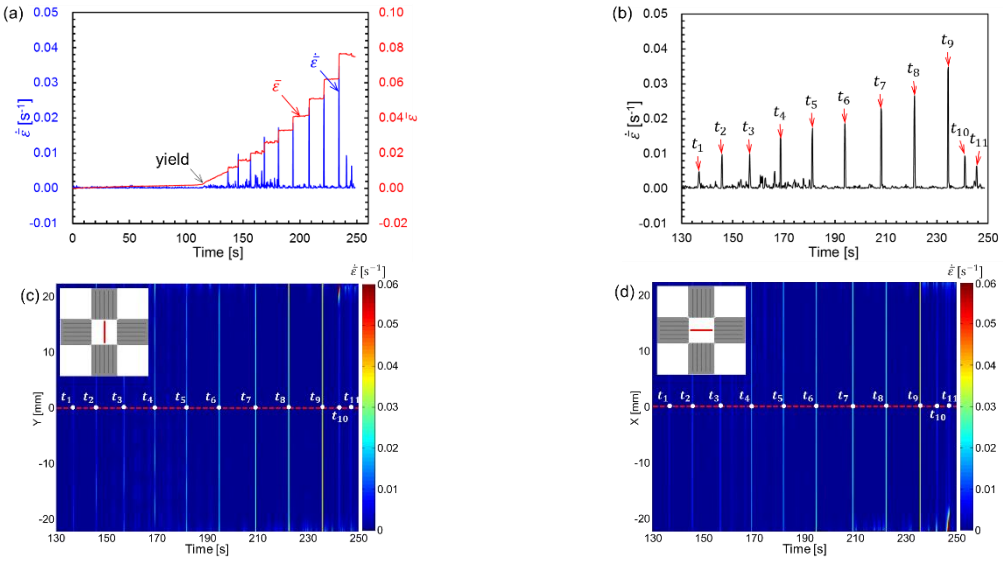


**Figure 8**. (a) The temporal evolution of $\dot{\bar{\varepsilon}}$ and $\bar{\varepsilon}$ at the geometrical center of cruciform specimen under equi-biaxial tension. (b) Spikes in evolution of $\dot{\bar{\varepsilon}}$. (c) The evolution of $\dot{\bar{\varepsilon}}$ contours along the geometrical central line in Y direction and (d) X direction under equi-biaxial tension.

The dramatic differences in spatio-temporal characteristics of plastic instabilities in AA5754-O under plane strain (X1Y2) and under equi-biaxial tension (X1Y1) are only caused by the different stress states.

The underlying microstructural mechanism needs to be explored in future work along with model modifications of existing theoretical frameworks to account for the influence of stress state.

## 4. Conclusions

Tensile tests of traditional uniaxial tensile specimens and optimized cruciform specimens of AA5754-O sheet were carried out with the aid of DIC techniques to investigate the different plastic instabilities under uniaxial tension, plane strain and equi-biaxial tension in the plane stress state. The Hockett-Sherby hardening law describes the hardening behavior of AA5754-O very well under these three stress states. Spatio-temporal characteristics of plastic instabilities exhibits compelling differences among the three stress states. Noted that these differences have not been previously reported in the literature. Yield point elongation (YPE) with initial yield stress of ~98 MPa is followed by stress serrations during hardening under uniaxial tension along DD and TD, however, YPE phenomenon doesn't appear in the hardening curve under uniaxial tension along RD. Unlike PLC behavior under uniaxial tension with a crossover of Type A to Type B serrations, AA5754-O deformed in the cruciform biaxial deformation exhibited very low amplitude serrations in flow curves under plane strain with YPE (X1Y2 specimen) and represents typical Type A serrations only after the equivalent plastic strain surpasses a critical level without YPE (X1Y1 specimen). These differences are a consequence of the different stress state, the geometry of the test specimens as well as the control mode of the testing program. The different PLC phenomena under uniaxial tension, plane strain and equi-biaxial tension requires improved models or modifications to existing theoretical frameworks for accurate forming simulation of Al-Mg alloy sheets.

## References

[1] Zhang F, Bower A F and Curtin W A 2012 The influence of serrated flow on necking in tensile specimens *Acta Mater.* **60** 43-50
[2] Lin Y C, Liu G, Chen M S, Li J, Zhou M and Zhou H M 2015 Effects of two-stage creep-aging processing on mechanical properties of an Al–Cu–Mg alloy *Materials & Design* **79** 127-35
[3] Lebyodkin M A, Kobelev N P, Bougherira Y, Entemeyer D, Fressengeas C, Gornakov V S, Lebedkina T A and Shashkov I V 2012 On the similarity of plastic flow processes during smooth and jerky flow: Statistical analysis *Acta Mater.* **60(9)** 3729-40
[4] Rodriguez P 1984 Serrated plastic flow *Bull. Mater. Sci.* **6(653-6)** 3
[5] Sarmah R and Ananthakrishna G 2015 Correlation between band propagation property and the nature of serrations in the Portevin–Le Châtelier effect. *Acta Mater.* **91** 192-201
[6] Manach P Y, Thuillier S, Yoon J W, Coër J and Laurent H 2014 Kinematics of Portevin–Le Chatelier bands in simple shear *Int. J. Plasticity* **58** 66-83
[7] Min J, Hector Jr L G, Carsley J E, Stoughton T B, Carlson B E and Lin J 2015 Spatio-temporal characteristics of plastic instability in AA5182-O during biaxial deformation *Materials & Design* **83** 786-94
[8] Sene N A, Balland P and Bouabdallah K 2018 Experimental study of Portevin–Le Châtelier bands on tensile and plane strain tensile tests *Archives Civil and Mech. Eng.* **18(1)** 94-102
[9] ISO 16842 2014 Metallic materials – sheet and strip – biaxial tensile testing method using a cruciform test piece
[10] Min J, Carsley J E, Lin J, Wen Y and Kuhlenkötter B 2016 A non-quadratic constitutive model under non-associated flow rule of sheet metals with anisotropic hardening: Modeling and experimental validation *Int. J. Mech. Sci.* **119** 343-59
[11] Hou Y, Min J, Lin J, Liu Z, Carsley J E and Stoughton T B 2017 Springback prediction of sheet metals using improved material models *Procedia Engineering* **207** 173-8

## Acknowledgments

Yong Hou would like to thank the generous support from General Motors Global Research & Development Center. Jianping Lin and Junying Min would like to acknowledge the financial support for this research provided through the GM collaborative research (GAC2214).